

Loss of Astrocyte Polarization in the Tg-ArcSwe Mouse Model of Alzheimer's Disease

Jing Yang^{a,b}, Lisa K. Lunde^b, Paworn Nuntagij^{b,c}, Tomohiro Oguchi^{b,d}, Laura M.A. Camassa^b, Lars N.G. Nilsson^e, Lars Lannfelt^e, Yuming Xu^a, Mahmood Amiry-Moghaddam^b, Ole Petter Ottersen^b and Reidun Torp^{b,*}

^aDepartment of Neurology, The First Affiliated Hospital of Zhengzhou University, Zhengzhou, P.R. China

^bCentre for Molecular Biology and Neuroscience, Department of Anatomy, Institute of Basic Medical Sciences, University of Oslo, Oslo, Norway

^cNeuro-Behavioural Biology Centre, Institute of Molecular Biosciences, Mahidol University, Mahidol, Thailand

^dDepartment of Otorhinolaryngology, Shinshu University of Medicine, Shinshu, Japan

^eDepartment of Public Health & Caring Sciences/Molecular Geriatrics, Uppsala University, Uppsala, Sweden

Accepted 20 July 2011

Abstract. Aquaporin-4 (AQP4) is the predominant water channel in brain and is selectively expressed in astrocytes. Astrocytic endfoot membranes exhibit tenfold higher densities of AQP4 than non-endfoot membranes, making AQP4 an excellent marker of astrocyte polarization. Loss of astrocyte polarization is known to compromise astrocytic function and to be associated with impaired water and K^+ homeostasis. Here we investigate by a combination of light and electron microscopic immunocytochemistry whether amyloid deposition is associated with a loss of astrocyte polarization, using AQP4 as a marker. We used the tg-ArcSwe mouse model of Alzheimer's disease, as this model displays perivascular plaques as well as plaques confined to the neuropil. 3D reconstructions were done to establish the spatial relation between plaques and astrocytic endfeet, the latter known to contain the perivascular pool of AQP4. Changes in AQP4 expression emerge just after the appearance of the first plaques. Typically, there is a loss of AQP4 from endfoot membranes at sites of perivascular amyloid deposits, combined with an upregulation of AQP4 in the neuropil surrounding plaques. By electron microscopy it could be verified that the upregulation reflects an increased concentration of AQP4 in those delicate astrocytic processes that abound in synaptic regions. Thus, astrocytes exhibit a redistribution of AQP4 from endfoot membranes to non-endfoot membrane domains. The present data suggest that the development of amyloid deposits is associated with a loss of astrocyte polarization. The possible perturbation of water and K^+ homeostasis could contribute to cognitive decline and seizure propensity in patients with Alzheimer's disease.

Keywords: Aquaporin-4, cerebral amyloid angiopathy, electron microscopy, immunocytochemistry, 3D reconstruction

INTRODUCTION

Scant information is available regarding the roles of astrocytes and astrocyte endfeet in the pathogenesis

and pathophysiology of Alzheimer's disease. This is surprising given the fact that astrocytes are essential in regulating transport across the brain-blood interface and in regulating homeostatic processes critical for neuronal function.

A perturbation of astrocytic function secondary to plaque formation and cerebral amyloid angiopathy (CAA) could interfere with synaptic processing and contribute to cognitive decline. Specifically, it remains

*Correspondence to: Reidun Torp, Centre for Molecular Biology and Neuroscience, Department of Anatomy, Institute of Basic Medical Sciences, University of Oslo, N-0317 Oslo, Norway. Tel.: +4722851269; Fax: +4722851278; E-mail: reidun.torp@medisin.uio.no.

to be resolved whether Alzheimer's disease is associated with a loss of astrocyte polarization. The term astrocyte polarization refers to the fact that astrocytes are endowed with processes that differ in regard to structure, function, and complement of membrane molecules [1]. Most notably, astrocytic processes abutting on cerebral microvessels or pia are characterized by a high density of the water channel AQP4 which is retained in these processes through interaction to the dystrophin associated protein complex (DAPC) [2–4]. The same processes are also enriched in the inwardly rectifying K^+ channel Kir 4.1, as shown in quantitative immunogold analyses of retinal Müller cells [5]. In contrast, astrocyte processes facing synaptic regions are enriched in glutamate transporters while the density of AQP4 is comparatively low [6–8]. A loss of astrocyte polarization may compromise the ability of astrocytes to regulate volume and water transport in the CNS and could also thwart K^+ siphoning which depends on the polarized expression of inwardly rectifying K^+ channels [9]. Animal models with loss of astrocyte polarity reveal delayed potassium clearance and increased seizure intensity [10]. Loss of astrocyte polarity has also been observed in human mesial temporal lobe epilepsy (MTLE) [11].

Here we use a combination of techniques to establish whether amyloid plaques, and perivascular amyloid deposits in particular, are associated with a perturbation of astrocyte endfeet leading to loss of astrocyte polarization. Electron microscopy provided the resolution required to resolve whether the endfeet were compromised by the amyloid aggregates while antibodies to AQP4 and dystrophin served as tools to assess astrocyte polarization. Our data indicate that the accumulation of amyloid in tg-ArcSwe mice is coupled temporally and spatially to loss of astrocyte polarization and a mislocalization and overexpression of AQP4 in non-endfoot membranes.

MATERIAL AND METHODS

Animal model and tissue preparation

Amyloid- β protein precursor (A β PP) transgenic mice harboring hA β PP with the Arctic (E693G) and Swedish (K670N, M671L) mutations (tg-ArcSwe mice) [12] and age-matched non-transgenic littermates were used in this study. All animal experiments were in accordance with the National Institutes of Health Guide for the care and use of laboratory animals and approved by the Biological Research

Ethics Committee in Norway. The animals used for immunofluorescence and electron microscopy were deeply anesthetized with Equithesin, transcardially perfused with 4% formaldehyde (PFA), post-fixed in 4% PFA overnight, and stored in 1/10 fixative at 4°C until further preparations. The animals used for Western blotting were decapitated, cerebral cortex dissected out and quickly frozen on dry ice and stored at –80°C until processed. Each age-group studied contained between 4–8 pairs of animals (tg-ArcSwe/wt). For electron microscopic analysis, pieces of cerebral cortex ($1.0 \times 0.5 \times 0.5 \text{ mm}^3$) were dissected from 500 μm -thick free floating sections under microscopy guidance (Olympus SZX12) and embedded in Lowicryl LM20 as described [13, 14]. There are two main steps in this procedure, cryoprotection and cryosubstitution. Cryoprotection was done by immersing the tissues into phosphate buffered glucose followed by increasing concentrations (10, 20, and 30%) of glycerol prior to plunging the tissue specimens into liquid propane at –190°C in a liquid nitrogen-cooled cryofixation unit KF80 (Reichert, Vienna, Austria). Cryosubstitution was undertaken in 0.5% uranyl acetate in anhydrous methanol at –90°C for 24 h in a cryosubstitution unit (AFS, Reichert). The temperature was stepwise increased to –45°C and Lowicryl HM20 was gradually substituted for methanol. Polymerization was performed under UV light for 48 h at –45°C.

Serial section and reconstruction

3D reconstruction of serial sections was described in our previous study [15]. In summary, serial sections of the Lowicryl-embedded tissue were cut with a diamond knife and placed on formvar-coated single-hole grids. Postembedding immunocytochemistry with 6E10 (or A β_{42}) antibody was used to identify amyloid deposits, and glutamine synthetase (GS) for astrocytic processes. Electron micrographs were obtained digitally from a transmission electron microscope with a camera. Analysis and 3D reconstruction were performed by Reconstruct, software specifically developed for serial section electron microscopy [16].

Antibodies and chemicals

6E10, the monoclonal (mouse) antibodies against amyloid- β -1-16 (Nordic BioSite) or polyclonal A β_{1-42} , (gift from UCI), polyclonal (rabbit) antibody against AQP4 (Chemicon and Sigma), polyclonal (chicken and rabbit) antibodies against GFAP (Nordic Biosite and Dako Cytomation), polyclonal antibody

Table 1

Exp.	Combination of 1st ab	Combination of 2nd ab
1.	AQP4: Millipore, rabbit, 1 : 1000 6E10: Nordic BioSite, mouse, 1 : 2000	Alex488: donkey anti rabbit, 1 : 1000 cy3: donkey anti mouse, 1 : 1000
2.	GFAP: Nordic Biosite, chicken, 1 : 1000 6E10: Nordic BioSite, mouse, 1 : 2000	cy3: donkey anti chicken, 1 : 1000 Alex488: donkey anti mouse, 1 : 1000
3.	AQP4: Millipore, rabbit, 1 : 800 6E10: Nordic BioSite, mouse, 1 : 2000 GFAP: Nordic Biosite, chicken, 1 : 500	cy3: donkey anti rabbit, 1 : 1000 Alex488: donkey anti mouse, 1 : 1000 cy5: donkey anti chicken, 1 : 1000
4.	AQP4: Millipore, rabbit, 1 : 800 6E10: Nordic BioSite, mouse, 1 : 2000 CD31: BD Biosciences, rat, 1 : 500	cy3: donkey anti rabbit, 1 : 1000 Alex: 488 donkey anti mouse, 1 : 1000 cy5: donkey anti rat, 1 : 1000
5.	Dystrophin: Abcam, rabbit, 1 : 500 6E10: Nordic BioSite, mouse, 1 : 2000 CD31: BD Biosciences, rat, 1 : 500	cy3: donkey anti rabbit, 1 : 1000 Alex488: donkey anti mouse, 1 : 1000 cy5: donkey anti rat, 1 : 1000

against glutamine synthetase (GS; Sigma), purified rat polyclonal antibody against CD31 (BD Biosciences), rabbit polyclonal anti-dystrophin antibody (Abcam), and anti-Beta-Actin antibody (Sigma) were used. Unless otherwise specified, all other chemicals were obtained from Sigma-Aldrich. For concentration of antibodies, see Tables 1 and 2.

Immunocytochemistry

Light microscopy

25 μ m-thick free-floating sections were cut by vibratome (Leica), pretreated in 90% formic acid, incubated in pre-incubation solution (10% NDS, 1% BSA, 0.5% Triton-X-100 in 0.01 M PBS) for 1 h at room temperature, then immunostained in primary antibody combinations (shown in Table 1) in primary incubation solution (3% NDS, 1% BSA, 0.5% Triton-X-100, 0.05% Sodium Acid in 0.01 M PBS) at 4°C overnight. After washing steps, the sections were incubated for 1 h at room temperature in the secondary antibody (shown in Table 1) diluted in 3% NDS, 1% BSA, 0.5% Triton-X-100 in 0.01 M PBS, then washed, and mounted on Superfrost-plus slides (Thermo Scientific) with Prolong Gold antifade reagent with DAPI (Invitrogen). Stored at -20°C in dark after drying. Images were taken by the Zeiss LSM5 PASCAL Confocal microscope.

Electron microscopy

The immunogold labeling was carried out according to the procedures by Matsubara et al. [17]. Briefly, the sections were incubated in 50 mM glycine in TBST (containing 5 mM Tris-HCl, 0.3% NaCl, 0.1% Triton X-100) for 10 min, followed by 2% human serum albumin (HSA) in TBST. The primary antibodies in 2% HSA in TBST were applied to the sections for

Table 2

Exp.	1st ab	2nd ab
1.	AQP4: Sigma, rabbit, 1 : 400	GAR-15 nm
2.	GFAP: Dako Cytomation, rabbit, 1 : 2000	GE healthcare, 1 : 20 GAR-15 nm
3.	6E10: Nordic BioSite, mouse, 1 : 1000 (anti-A β ₄₂ gift from UCI, 1 : 500)	Abcam, 1 : 20 GAM-10 or 15 nm
4.	GS: Sigma, rabbit, 1 : 300	Abcam, 1 : 20 GAR-15 nm Abcam, 1 : 20
5.	AQP4 and 6E10 AQP4 and GFAP AQP4 and GS	GAR-20 nm and GFAM-10 nm Abcam and BBI, 1 : 20

2 h (anti-AQP4 1 : 300, 6E10 1 : 1000, anti-GS 1 : 300, anti-GFAP 1 : 2000). The sections were then rinsed twice by TBST before being incubated with goat anti-rabbit or anti-mouse Fab fragments coupled to gold particles (Table 2) in 2% HSA TBST for 1 h. Double labeling was achieved by incubating tissue section with both monoclonal and polyclonal antibodies or using formaldehyde vapor at 80°C for 1 h before applying the next round of immune-incubation if the antibodies were of the same types. For enhancing the contrast, uranyl acetate (Fluorochem) in double distilled water and lead citrate were used. The labeling was examined in a transmission electron microscope (TECNAI 12).

Western blot

Protein concentrations were determined with a DC protein assay (Bio-Rad). After diluting the samples in loading buffer (0.875% SDS, 5% Glycerol, 50 mM Tris-HCl pH 6.8, 0.83% β -mercaptoethanol and trace amount of bromophenol blue), 2 μ g of protein was

added per lane, separated by electrophoresis on 12.5% polyacrylamide gels (Criterion Precast Gel, Bio-Rad) and transferred onto PVDF membranes (Criterion gel blotting sandwich, Bio-Rad). Membranes were blocked for 2 h in Tris-buffered saline (20 mM Tris, 137 mM NaCl) plus 0.1% Tween (TBS-T) and 5% skim milk powder (Sigma-Aldrich) followed by overnight incubation in primary antibody (see antibodies) diluted in TBS-T with 5% skim milk powder.

Membranes were subsequently incubated for 1 h in secondary antibody (Sigma-Aldrich) diluted 1 : 10000 in TBS-T and detected with the ECF kit according to the manufacturer's instructions (GE Healthcare). All steps were carried out at room temperature and after each step membranes were washed in TBS-T.

RESULTS

The tg-ArcSwe model is known to develop amyloid plaques in brain neuropil. By electron microscopy we could show that A β was associated with brain microvessels (Fig. 1). The deposits were identified by antibodies recognizing A β ₄₂ [15]. By use of a series of ultrathin sections subjected to immunogold labeling for A β ₄₂, the amyloid deposits were reconstructed in order to display their relation to cells and processes at the brain-blood interface. A β deposits impinged directly on the perivascular astrocyte endfeet (Fig. 1E, also see Fig. 4) and in many occasions extended to the endothelial basal lamina, thus separating the astrocyte processes that normally form a continuous sheath around brain microvessels [18].

Using double immunofluorescence labeling, we assessed whether the development of plaques was temporally and spatially coupled to changes in AQP4 expression. At 4 months of age, when only small and largely intracellular aggregates of A β were present (Fig. 2B), the distribution of AQP4 was qualitatively and quantitatively similar to that seen in wild-type animals (Fig. 2A). Specifically, the AQP4 immunosignal was confined to the brain-blood interface. At 8 months, CAA was commonly observed around brain microvessels (Fig. 2C-D).

Microvessels associated with CAA did not display significant AQP4 labeling (Fig. 2C-F; also see Fig. 6). The loss of perivascular AQP4 immunolabeling was not a function of age as brain microvessels devoid of amyloid retained a strong AQP4 immunosignal (arrow, Fig. 2C-D). Nor could the loss of perivascular AQP4 be explained by retraction of astrocyte processes as GFAP

immunolabeling confirmed that astrocyte processes were intact (Fig. 2D; also see Fig. 4). At 12 and 16 months of age, there was an increasing accumulation of amyloid around small brain vessels (Fig. 2E-F). Concurrently, the perivascular immunosignal for AQP4 decreased, compared with the signal recorded at 4 months or in wild-type animals (Fig. 2A-B).

While perivascular AQP4 labeling decreased with progression of disease, the neuropil AQP4 labeling increased (Fig. 2). The increase in AQP4 labeling was particularly pronounced in the neuropil abluminal to the perivascular plaques (Fig. 2C and D).

The changes observed in the immunofluorescence preparations were confirmed at the electron microscopic level (Figs. 3 and 4). The distinct perivascular AQP4 signal typical of wild-type animals (Fig. 3A) stood in sharp contrast to the patchy labeling in the transgenic animals. Notably, there were few particles immunopositive for AQP4 at sites where the amyloid deposits touched the astrocyte processes or the endothelial basal lamina (Fig. 3B, 4D). Figure 4 shows that vessels devoid of CAA retain their complement of AQP4 while contiguous amyloid-laden vessels have lost their perivascular AQP4 pool.

Electron microscopic analysis also confirmed the light microscopic data indicating an increased neuropil labeling in the transgenic animals (compare Fig. 3A with Fig. 3C). The enhanced AQP4 immunogold in the neuropil could be attributed to an increased labeling density of GFAP immunopositive profiles, suggestive of a redistribution of labeling from perivascular astrocyte processes to astrocyte processes contacting neuronal elements in the neuropil.

To corroborate the immunocytochemical data indicating increased AQP4 immunolabeling in neuropil of transgenic animals (Figs. 2 and 3), we performed a Western blot analysis. This analysis showed that the level of AQP4 protein was significantly higher in AD animals than in wild-type controls (Fig. 5). In the transgenic animals, the amount of AQP4 (recorded in frontal cortex) was higher at 9 months of age than at 16 months. Endfoot astrocytic membranes only constitute a small membrane fraction compared with the astrocytic membranes in the neuropil. Thus the Western blot signals reflect the size of the AQP4 pool in the latter membranes.

Aquaporin-4 is anchored in perivascular membranes through binding to the dystrophin associated protein complex [2]. Similar to AQP4, dystrophin was lost from those vessels that accumulated amyloid deposits (Fig. 6).

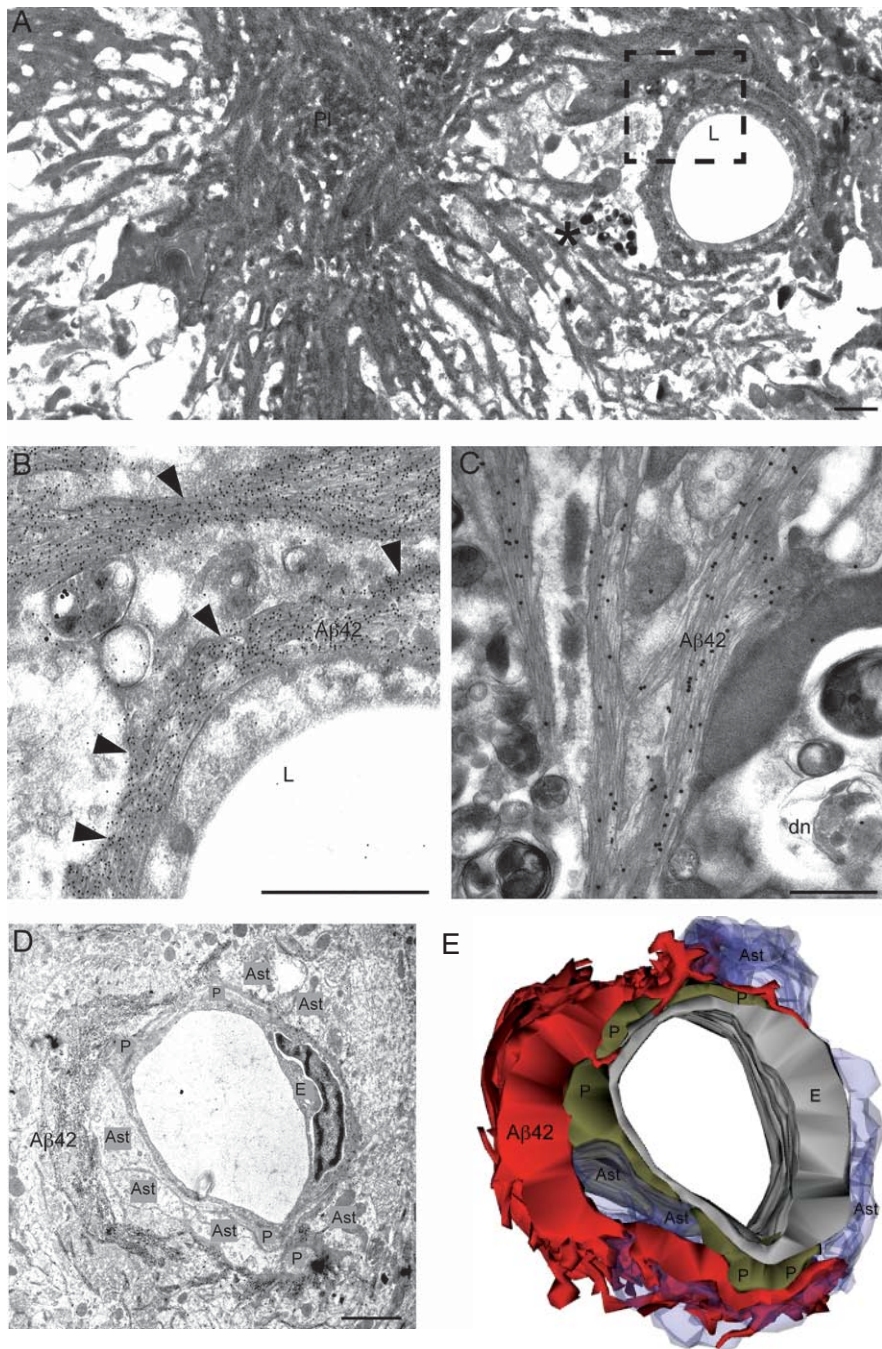


Fig. 1. Electron micrograph of A β ₄₂ immunopositive deposit in tg-A β PP-ArcSwe mouse cortex (A). The plaque (Pl) is of considerable size with radiating fibrils. The fibrils are decorating a nearby vessel (L, vessel lumen). The plaque is associated with dystrophic neurites. To appreciate the immunogold labeling, two areas (indicated with box and star, respectively) are enlarged in B and C. In B, the fibrillar deposit is indicated by arrowheads; in C, the dystrophic neurites (dn) are clearly visible. A β deposits (immuno-positive for A β ₄₂) were found in the extracellular space around the astrocyte endfoot-endothelial complex, including pericyte processes, astrocyte endfoot processes, and endothelial cells (D). E) The 3D reconstruction shows that A β ₄₂ deposits touch several structures of this complex. No breakage of the endothelial lining was observed in the serial sections included in this study. The basal lamina still covers the entire abluminal surface of the capillary endothelium, separating A β ₄₂ deposits from the endothelial lining. The astrocytic endfoot covering is interrupted by A β deposits. Abbreviations: Ast, astrocyte processes; E, endothelial cell; P, pericytes. Scale bars, 0.5 μ m in A-C and 0.3 μ m in D.

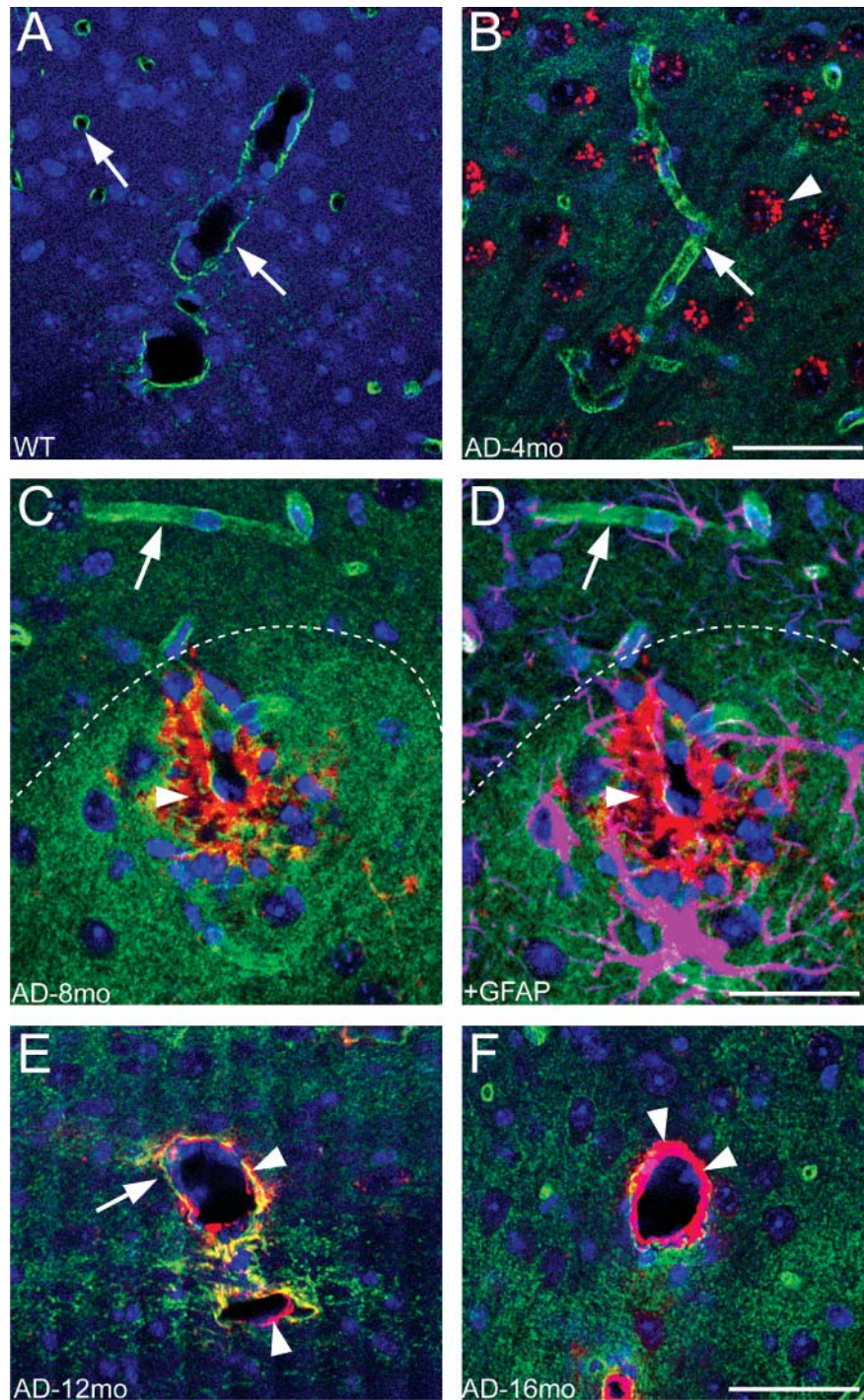


Fig. 2. Immunoreactive A β aggregates (red) was first seen at 4 months in AD mice (B), and peaked at 8–16 months when severe extracellular plaque deposition was apparent (C–F) in association with infiltration of GFAP-immunoreactive astrocytes (purple; D). Deposits around the vessels were invariably associated with an increase in AQP4 immunofluorescence (green) in the neuropil (C–F), showing loss of polarity compared to the normal distribution of AQP4 (A). Small vessels covered by A β lost their linear labeling of AQPs. However, AQP4 immunolabeling was dense in glial membranes in close vicinity to the affected vessels, highlighted in C and D and indicated by the lines. The arrows in A, B, C, and D point to endfeet with a normal distribution of AQP4. Arrowheads point to A β deposits (B,C,D,E,F). Arrow in E indicates a site where AQP4 persists. All sections were counterstained with DAPI (blue) featuring the nuclei. Scale bars, 50 μ m.

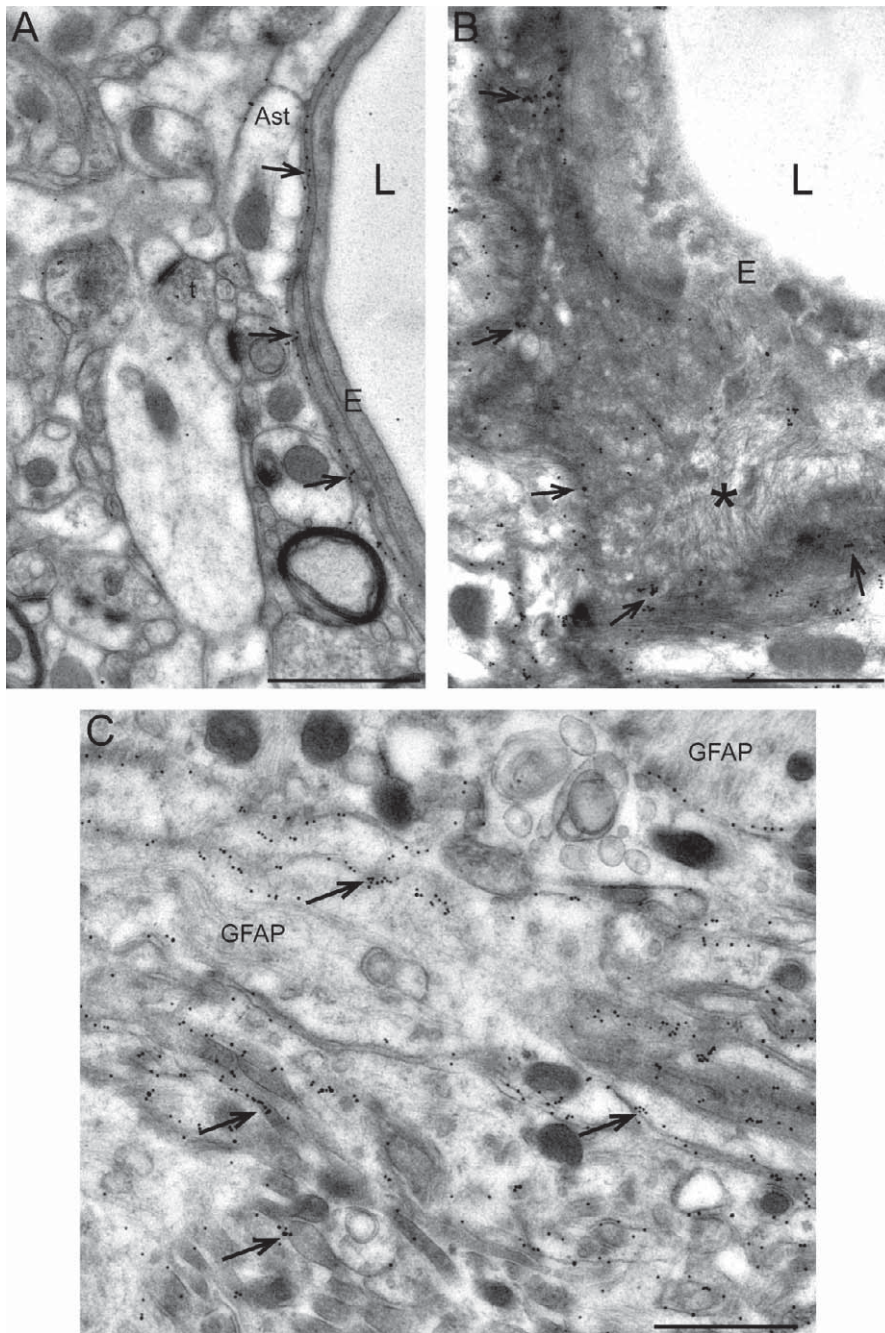


Fig. 3. Electron micrographs show how A β deposition is associated with loss of astrocytic polarity at 8 months. A) Normal linear distribution of AQP4 in wild type, gold particles indicated by arrows. B) AQP4 (gold particles indicated by arrows) lose their polarity as A β (asterisk) accumulates around the vessel (CAA). C) Increase in AQP4-immunoreactivity in the non-endfeet membranes, indicated by arrows. (Compare with wild type littermate in A) Abbreviations: Ast, astrocyte; E, endothelial cell; GFAP, glial fibrillary acidic protein; L, lumen. Scale bars, 0.5 μ m.

DISCUSSION

The present data indicate that the development of amyloid deposits in tg-ArcSwe mice is associated with

a loss of astrocyte polarization. Our time course analysis suggests that loss of astrocyte polarization is a consequence rather than cause of A β deposition. The data are consistent with the idea that aggregation of

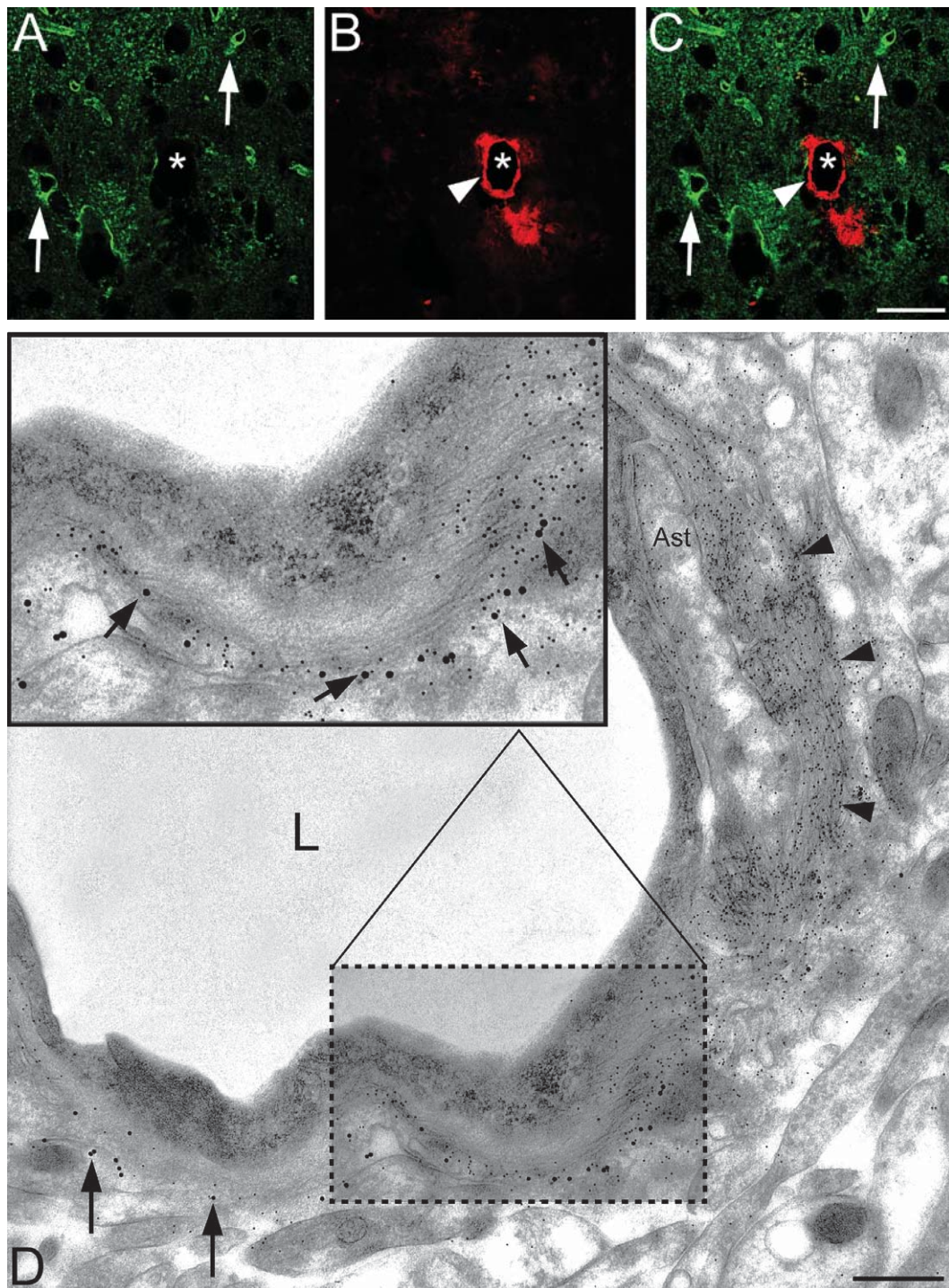


Fig. 4. Close relationship between A β deposition and down regulation of AQP4 labeling. Sites of large amyloid deposits (CAA) are characterized by a mislocalization of AQP4 as shown by confocal microscopy (A,B,C). Asterisk indicates vessel where AQP4 is lost (AQP4, green) and arrows point to normal AQP4 distribution. Arrowhead in B and C indicate A β deposits around a vessel (red). D) High magnification of the close relationship between amyloid and AQP4. Where A β occurs (small gold particles and arrowheads), AQP4 is lost from the endfeet (big gold particles). Where amyloid is absent, the linear labeling for AQP4 is maintained (arrows). The insert represents a closer view of the relationship between these players. Abbreviations: Ast, astrocyte, L, lumen. Scale bars, LM 50 μ m, EM 0.5 μ m.

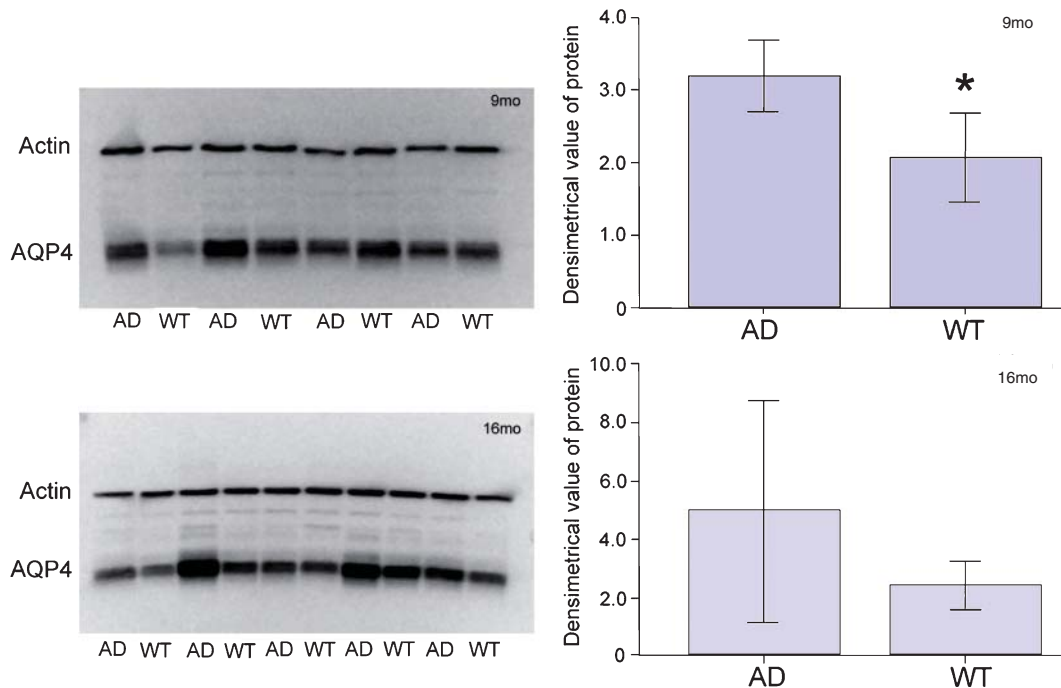


Fig. 5. SDS-Page and Western blot from frontal cortex homogenates show a significant increase in the AQP4 expression in tg-ArcSwe mice at the age of 9 months compared to wild type ($p < 0.05$, $n = 8$). This difference was attenuated at the age of 16 months, although it did not reach statistical significance $p > 0.05$, $n = 10$, Independent T-test, Error bars ± 2 SE.

A β disrupts the perivascular sheath of astrocyte processes and interferes with the mechanisms that are normally responsible for the anchoring of the perivascular AQP4 pool. As changes in dystrophin expression parallel the changes in AQP4 expression, the most salient explanation is that amyloid deposition coincides in time with activation of extracellular proteases. Thus, extracellular proteases may cleave the dystroglycan bridge that serves to attach the dystrophin associated protein complex to the basal lamina. Matrix metalloproteinases are obvious candidates. A number of studies concur to demonstrate increased metalloproteinase activity in Alzheimer's disease and several of the metalloproteinases in question are known to target beta-dystroglycan [19–22].

Loss of astrocyte polarization is likely to have significant impact on brain function. Astrocytes are endowed with specialized membrane domains that reflect the multitude of spatially restricted tasks that the astrocytes normally subservise. Potassium siphoning is an example of such a task. As originally defined [23], potassium siphoning is a special case of K^+ spatial buffering that helps clear excess K^+ from synaptic regions by redistribution to distant sites. Studies in Müller cells revealed much higher K^+ conductances in endfeet membranes than in membranes opposed to

synaptic regions, supporting the idea that K^+ taken up in synaptic regions is "siphoned" through the endfeet membranes [24]. Immunocytochemical data support this idea, by demonstrating a tenfold higher density of the inwardly rectifying K^+ channel Kir 4.1 in endfeet membranes than in non-endfeet membrane domains [5]. The distribution of Kir 4.1 mirrored the distribution of AQP4, leading to the hypothesis that AQP4 mediated water transport accompanies K^+ redistribution [1]. Indeed, animals suffering a loss of AQP4 from astrocytic endfeet following targeted deletion of alpha-syntrophin show delayed clearance of K^+ from the extracellular space [10]. Deletion of alpha-syntrophin (which serves to anchor AQP4 in endfeet membranes) leads to a redistribution of AQP4 along the astrocytic membrane [10], mimicking the changes in AQP4 expression presently observed in the tg-ArcSwe model.

Analyses of glutamate transporters were beyond the scope of the present study. But it should be emphasized that the distribution of such transporters shows a polarity opposite to that of AQP4. Thus while the glutamate transporter EAAT1 is enriched in those astrocyte membranes that abut on excitatory synapses, it is weakly expressed in those endfeet membranes that contain high densities of AQP4 [6]. If loss of astrocyte polarity is generalized so as to also involve glutamate

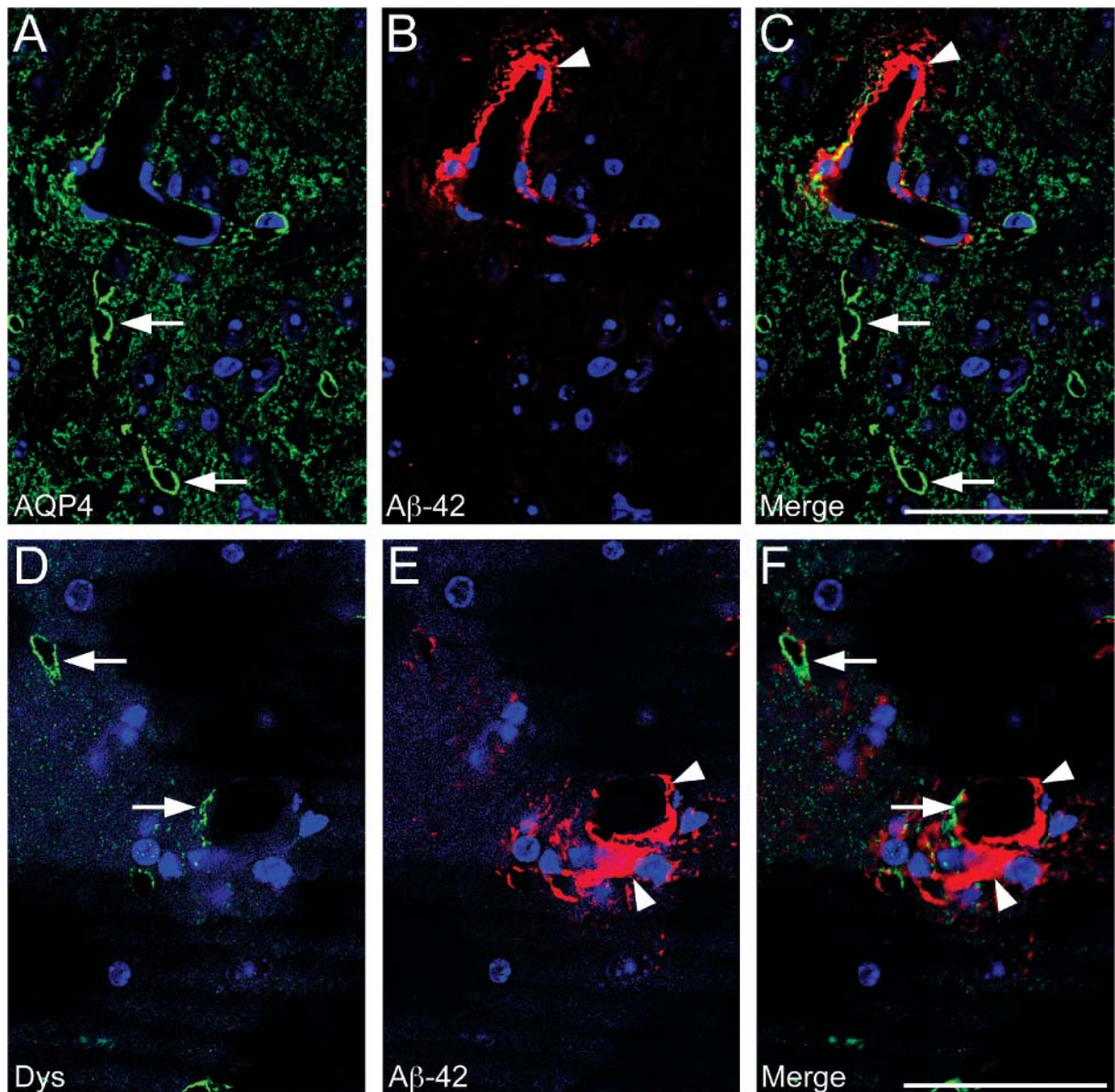


Fig. 6. Immunofluorescent images show loss of perivascular AQP4 (A-C) and dystrophin-associated protein complex immunoreactivity (D-F) in the areas with amyloid angiopathy (arrowhead; B-C and E-F). Note that the smaller vessels and capillaries, which are not affected by the amyloid deposits stain positive for perivascular AQP4 and dystrophin (green and arrows). Scale bars, 50 μ m.

transporters, this would imply that glutamate clearance would be less efficient than normal. The changes presently observed imply that astrocytes are impaired when it comes to the homeostatic functions that they normally subserve.

It has long been known that patients with Alzheimer's disease are predisposed to epileptic seizures [25–29]. Similarly, non-convulsive seizure activity has been demonstrated in A β PP transgenic mice [30]. As yet, no mechanisms have been identified

to underpin this association. Loss of astrocyte polarity might provide the link. Thus, mice with targeted deletion of alpha-syntrophin [2] (known to anchor AQP4 to endfoot membranes) show a loss of astrocytic polarization similar to that found in the present material and exhibit increased severity of seizures compared with wild-type animals [10, 31]. Loss of astrocyte polarization (reflected as a loss of perivascular AQP4) is also found in the sclerotic hippocampi of patients with mesial temporal lobe sclerosis [11]. By extrapo-

lation, the loss of astrocyte polarization unraveled in the present animals may be indicative of a perturbed K^+ spatial buffering that in turn may predispose for hyperexcitability and epileptic seizures.

The ratio between $A\beta_{42}$ and $A\beta_{40}$ in the present mouse model [32] may not be representative of that in humans where $A\beta_{40}$ may be relatively more abundant, depending, i.e., on apolipoprotein status [33–35]. This calls for caution when extrapolations are made from the present Alzheimer's disease model to the clinical condition.

In conclusion, the present data suggest that perivascular $A\beta_{42}$ deposits may be particularly deleterious to brain function as they by compromising endfoot function also will interfere with the homeostatic functions of astrocytes at large. Our findings introduce a new dimension to the understanding of the pathophysiology and pathogenesis of Alzheimer's disease.

ACKNOWLEDGMENTS

Jing Yang was supported through a joint grant from the Medical Scholars Program, Zhengzhou University and University of Oslo. We thank Professor F.M. Haug for all the efforts of interpreting our EM data. The work was supported by Civitan Norway (Alzheimer task force), the Research Council of Norway, and Polish-Norwegian Research Fund grant PNRF-96 and The Swedish Research Council (2009–4567, LL, 2009–4389, LN). The Uppsala University Transgenic Facility (UUTF) is greatly acknowledged for helping in developing the tg-ArcSwe transgenic model.

Authors' disclosures available online (<http://www.j-alz.com/disclosures/view.php?id=950>).

REFERENCES

- [1] Amiry-Moghaddam M, Ottersen OP (2003) The molecular basis of water transport in the brain. *Nat Rev Neurosci* **4**, 991-1001.
- [2] Neely JD, Amiry-Moghaddam M, Ottersen OP, Froehner SC, Agre P, Adams ME (2001) Syntrophin-dependent expression and localization of Aquaporin-4 water channel protein. *Proc Natl Acad Sci U S A* **98**, 14108-14113.
- [3] Amiry-Moghaddam M, Frydenlund DS, Ottersen OP (2004) Anchoring of aquaporin-4 in brain: Molecular mechanisms and implications for the physiology and pathophysiology of water transport. *Neuroscience* **129**, 999-1010.
- [4] Amiry-Moghaddam M, Otsuka T, Hurn PD, Traystman RJ, Haug FM, Froehner SC, Adams ME, Neely JD, Agre P, Ottersen OP, Bhardwaj A (2003) An alpha-syntrophin-dependent pool of AQP4 in astroglial end-feet confers bidirectional water flow between blood and brain. *Proc Natl Acad Sci U S A* **100**, 2106-2111.
- [5] Nagelhus EA, Horio Y, Inanobe A, Fujita A, Haug FM, Nielsen S, Kurachi Y, Ottersen OP (1999) Immunogold evidence suggests that coupling of K^+ siphoning and water transport in rat retinal Müller cells is mediated by a co-enrichment of Kir4.1 and AQP4 in specific membrane domains. *Glia* **26**, 47-54.
- [6] Nagelhus EA, Veruki ML, Torp R, Haug FM, Laake JH, Nielsen S, Agre P, Ottersen OP (1998) Aquaporin-4 water channel protein in the rat retina and optic nerve: Polarized expression in Müller cells and fibrous astrocytes. *J Neurosci* **18**, 2506-2519.
- [7] Nielsen S, Nagelhus EA, Amiry-Moghaddam M, Bourque C, Agre P, Ottersen OP (1997) Specialized membrane domains for water transport in glial cells: High-resolution immunogold cytochemistry of aquaporin-4 in rat brain. *J Neurosci* **17**, 171-180.
- [8] Chaudhry FA, Lehre KP, van Lookeren Campagne M, Ottersen OP, Danbolt NC, Storm-Mathisen J (1995) Glutamate transporters in glial plasma membranes: Highly differentiated localizations revealed by quantitative ultrastructural immunocytochemistry. *Neuron* **15**, 711-720.
- [9] Kofuji P, Newman EA (2004) Potassium buffering in the central nervous system. *Neuroscience* **129**, 1045-1056.
- [10] Amiry-Moghaddam M, Williamson A, Palomba M, Eid T, de Lanerolle NC, Nagelhus EA, Adams ME, Froehner SC, Agre P, Ottersen OP (2003) Delayed K^+ clearance associated with aquaporin-4 mislocalization: Phenotypic defects in brains of alpha-syntrophin-null mice. *Proc Natl Acad Sci U S A* **100**, 13615-13620.
- [11] Eid T, Lee TS, Thomas MJ, Amiry-Moghaddam M, Bjørnsen LP, Spencer DD, Agre P, Ottersen OP, de Lanerolle NC (2005) Loss of perivascular aquaporin 4 may underlie deficient water and K^+ homeostasis in the human epileptogenic hippocampus. *Proc Natl Acad Sci U S A* **102**, 1193-1198.
- [12] Lord A, Kalimo H, Eckman C, Zhang XQ, Lannfelt L, Nilsson LN (2006) The Arctic Alzheimer mutation facilitates early intraneuronal Abeta aggregation and senile plaque. *Neurobiol Aging* **27**, 67-77.
- [13] Takumi Y, Ramirez-León V, Laake P, Rinvik E, Ottersen OP (1999) Different modes of expression of AMPA and NMDA receptors in hippocampal synapses. *Nat Neurosci* **2**, 618-624.
- [14] Torp R, Head E, Milgram NW, Hahn F, Ottersen OP, Cotman CW (2000) Ultrastructural evidence of fibrillar beta-amyloid associated with neuronal membranes in behaviorally characterized aged dog brains. *Neuroscience* **96**, 495-506.
- [15] Nuntagij P, Oddo S, LaFerla FM, Kotchabhakdi N, Ottersen OP, Torp R (2009) Amyloid deposits show complexity and intimate spatial relationship with dendrosomatic plasma membranes: An electron microscopic 3D reconstruction analysis in 3xTg-AD mice and aged canines. *J Alzheimers Dis* **16**, 315-323.
- [16] Fiala JC (2005) Reconstruct: A free editor for serial section microscopy. *J Microsc* **218**, 52-61.
- [17] Matsubara A, Takumi Y, Nakagawa T, Usami S, Shinkawa H, Ottersen OP (1999) Immunoelectron microscopy of AMPA receptor subunits reveals three types of putative glutamatergic synapse in the rat vestibular end organs. *Brain Res* **819**, 58-64.
- [18] Mathiesen TM, Lehre KP, Danbolt NC, Ottersen OP (2010) The perivascular astroglial sheath provides a complete covering of the brain microvessels: an electron microscopic 3D reconstruction. *Glia* **58**, 1094-1103.
- [19] Leake A, Morris CM, Whateley J (2000) Brain matrix metalloproteinase 1 levels are elevated in Alzheimer's disease. *Neurosci Lett* **291**, 201-203.

- [20] Adair JC, Charlie J, Dencoff JE, Kaye JA, Quinn JF, Camicioli RM, Stetler-Stevenson WG, Rosenberg GA (2004) Measurement of gelatinase B (MMP-9) in the cerebrospinal fluid of patients with vascular dementia and Alzheimer disease. *Stroke* **35**, e159-e162.
- [21] Yamada H, Saito F, Fukuta-Ohi H, Zhong D, Hase A, Arai K, Okuyama A, Maekawa R, Shimizu T, Matsumura K (2001) Processing of beta-dystroglycan by matrix metalloproteinase disrupts the link between the extracellular matrix and cell membrane via the dystroglycan complex. *Hum Mol Genet* **10**, 1563-1569.
- [22] Michaluk P, Kolodziej L, Mioduszevska B, Wilczynski GM, Dzwonek J, Jaworski J, Gorecki DC, Ottersen OP, Kaczmarek L (2007) Beta-dystroglycan as a target for MMP-9, in response to enhanced neuronal activity. *J Biol Chem* **282**, 16036-16041.
- [23] Paulson OB, Newman EA (1987) Does the release of potassium from astrocyte endfeet regulate cerebral blood flow? *Science* **237**, 896-898.
- [24] Newman EA (2004) Glial modulation of synaptic transmission in the retina. *Glia* **47**, 268-274.
- [25] Hesdorffer DC, Hauser WA, Annegers JF, Kokmen E, Rocca WA (1996) Dementia and adult-onset unprovoked seizures. *Neurology* **46**, 727-730.
- [26] Hauser WA, Morris ML, Heston LL, Anderson VE (1986) Seizures and myoclonus in patients with Alzheimer's disease. *Neurology* **36**, 1226-1230.
- [27] Romanelli MF, Morris JC, Ashkin K, Coben LA (1990) Advanced Alzheimer's disease is a risk factor for late-onset seizures. *Arch Neurol* **47**, 847-850.
- [28] Amatniek JC, Hauser WA, DelCastillo-Castaneda C, Jacobs DM, Marder K, Bell K, Albert M, Brandt J, Stern Y (2006) Incidence and predictors of seizures in patients with Alzheimer's disease. *Epilepsia* **47**, 867-872.
- [29] Palop JJ, Mucke L (2009) Epilepsy and cognitive impairments in Alzheimer disease. *Arch Neurol* **66**, 435-440.
- [30] Palop JJ, Chin J, Roberson ED, Wang J, Thwin MT, Bien-Ly N, Yoo J, Ho KO, Yu GQ, Kreitzer A, Finkbeiner S, Noebels JL, Mucke L (2007) Aberrant excitatory neuronal activity and compensatory remodeling of inhibitory hippocampal circuits in mouse models of Alzheimer's disease. *Neuron* **55**, 697-711.
- [31] Bragg AD, Amiry-Moghaddam M, Ottersen OP, Adams ME, Froehner SC (2006) Assembly of a perivascular astrocyte protein scaffold at the mammalian blood-brain barrier is dependent on alpha-syntrophin. *Glia* **53**, 879-890.
- [32] Philipson O, Hammarström P, Nilsson KP, Portelius E, Olofsson T, Ingelsson M, Hyman BT, Blennow K, Lannfelt L, Kalimo H, Nilsson LN (2009) A highly insoluble state of Abeta similar to that of Alzheimer's disease brain is found in Arctic APP transgenic mice. *Neurobiol Aging* **30**, 1393-1405.
- [33] Schmechel DE, Saunders AM, Strittmatter WJ, Crain BJ, Hulette CM, Joo SH, Pericak-Vance MA, Goldgaber D, Roses AD (1993) Increased amyloid beta-peptide deposition in cerebral cortex as a consequence of apolipoprotein E genotype in late-onset Alzheimer disease. *Proc Natl Acad Sci U S A* **90**, 9649-9653.
- [34] Thal DR, Papassotiropoulos A, Saïdo TC, Griffin WS, Mrak RE, Kölsch H, Del Tredici K, Attems J, Ghebremedhin E (2010) Capillary cerebral amyloid angiopathy identifies a distinct APOE epsilon4-associated subtype of sporadic Alzheimer's disease. *Acta Neuropathol* **120**, 169-183.
- [35] Fryer JD, Simmons K, Parsadanian M, Bales KR, Paul SM, Sullivan PM, Holtzman DM (2005) Human apolipoprotein E4 alters the amyloid-beta 40:42 ratio and promotes the formation of cerebral amyloid angiopathy in an amyloid precursor protein transgenic model. *J Neurosci* **25**, 2803-2810.